Original

Null mutation of exocyst complex component 3-like does not affect vascular development in mice

Satsuki TAKASHIMA[1], Eiichi OKAMURA[1], Yusuke ICHIYAMA[2], Kiyoto NISHI[3], Akio SHIMIZU[4], Chisato WATANABE[1], Masanaga MUTO[1], Shoma MATSUMOTO[1], Setsuko TSUKIYAMA-FUJII[1], Tomoyuki TSUKIYAMA[1], Hisakazu OGITA[4], Eiichiro NISHI[3], Masahito OHJI[2], Fumihiro SUGIYAMA[5], Satoru TAKAHASHI[5–7], Seiya MIZUNO[5], Ken-ichi MIZUTANI[8] and Masatsugu EMA[1]

[1]Department of Stem Cells and Human Disease Models, Research Center for Animal Life Science, Shiga University of Medical Science, Seta, Tsukinowa-cho, Otsu, Shiga 520-2192, Japan
[2]Department of Ophthalmology, Shiga University of Medical Science, Seta, Tsukinowa-cho, Otsu, Shiga 520-2192, Japan
[3]Department of Pharmacology, Shiga University of Medical Science, Seta, Tsukinowa-cho, Otsu, Shiga 520-2192, Japan
[4]Division of Molecular Medical Biochemistry, Department of Biochemistry and Molecular Biology, Shiga University of Medical Science, Seta, Tsukinowa-cho, Otsu, Shiga 520-2192, Japan
[5]Laboratory Animal Resource Center in Transborder Medical Research Center, University of Tsukuba, 1-1-1 Tennodai, Tsukuba, Ibaraki 305-8577, Japan
[6]Department of Anatomy and Embryology, Faculty of Medicine, University of Tsukuba, 1-1-1 Tennodai, Tsukuba, Ibaraki 305-8577, Japan
[7]International Institute for Integrative Sleep Medicine (WPI-IIIS), University of Tsukuba, 1-1-1 Tennodai, Tsukuba, Ibaraki 305-8577, Japan
[8]Laboratory of Stem Cell Biology, Graduate School of Pharmaceutical Sciences, Kobe Gakuin University, 1-1-3 Minatojima, Chuo-ku, Kobe, Hyogo 650-8586, Japan

Abstract: Exocyst is an octameric protein complex implicated in exocytosis. The exocyst complex is highly conserved among mammalian species, but the physiological function of each subunit in exocyst remains unclear. Previously, we identified exocyst complex component 3-like (*Exoc3l*) as a gene abundantly expressed in embryonic endothelial cells and implicated in the process of angiogenesis in human umbilical cord endothelial cells. Here, to reveal the physiological roles of *Exoc3l* during development, we generated *Exoc3l* knockout (KO) mice by genome editing with CRISPR/Cas9. *Exoc3l* KO mice were viable and showed no significant phenotype in embryonic angiogenesis or postnatal retinal angiogenesis. *Exoc3l* KO mice also showed no significant alteration in cholesterol homeostasis or insulin secretion, although several reports suggest an association of *Exoc3l* with these processes. Despite the implied roles, *Exoc3l* KO mice exhibited no apparent phenotype in vascular development, cholesterol homeostasis, or insulin secretion.
Key words: cardiovascular development, cholesterol, exocyst complex, exocyst complex component 3-like, insulin secretion

Introduction

Angiogenesis is new blood vessel formation from pre-existing endothelial cells and plays major roles in physiological processes, such as embryonic development, tissue regeneration, and ovulation, as well as pathological processes such as tumorigenesis [1, 2]. In response to vascular endothelial growth factor (VEGF)-A, a specialized endothelial cell type called a tip cell extends filopodia at the forefront of vascular structures to guide

migration [3]. Stalk cells localize behind tip cells and proliferate more rapidly to extend vascular structures [3]. These processes are coordinated by many autocrine and paracrine signaling factors, shear stress, and metabolites [1, 2].

Exocyst is a multimeric protein complex that controls exocytosis by tethering vesicles to the plasma membrane and regulates cadherin trafficking from recycling endosomes to plasma membranes, cadherin clustering [4], epithelial polarization [5], Notch signaling, and primary ciliogenesis [6]. The exocyst complex consists of eight subunits. Exoc1–Exoc8 subunits are highly conserved from yeast to humans. Knockout (KO) of some subunits leads to early embryonic lethality with various phenotypes [7–10]. *Exoc3* has four homologous genes in vertebrates, called *Exoc3-like (Exoc3l), Exoc3-like 2 (Exoc3l2), Exoc3-like 3 (Exoc3l3)*, and *Exoc3-like 4 (Exoc3l4). Exoc3l2* is abundantly expressed in embryonic endothelial cells. *Exoc3l2* KO mice show early embryonic lethality with cardiovascular defects and brain abnormalities [11]. As the exocyst complex is also implicated in vesicle trafficking, it may affect various developmental processes in a paracrine manner.

A previous Meta analysis has indicated that *EXOC3L1*, a human ortholog of *Exoc3l* is associated with HDL concentration [12]. Saito *et al*. reported that *Exoc3l* protein forms a complex with Exoc4 and is implicated in insulin secretion on the basis of *in vitro* experiments [13]. Takase and coworker indicated that *Exoc3l* is an endothelial cell-enriched gene during mouse embryonic development and knockdown of *EXOC3l*, causes a severe defect in VEGF-A-dependent angiogenesis in human umbilical vein endothelial cells (HUVEC) [14]. However, the physiological function of *Exoc3l* in mice remains largely unknown.

In this study, we generated *Exoc3l* KO mice by genome editing with CRISPR/Cas9 and found that *Exoc3l* KO mice were viable until adulthood without any phenotypic manifestations. *Exoc3l* KO mice showed no significant alteration in angiogenesis during embryonic development or in postnatal retinal development. *Exoc3l* KO mice also showed no significant change in cholesterol homeostasis or insulin secretion. Thus, *Exoc3l* KO mice exhibited no apparent phenotype in vascular development, cholesterol homeostasis, or insulin secretion, despite the suggested roles.

Materials and Methods

Animals

Exoc3l KO mice were generated at the animal facility in the University of Tsukuba. Briefly, 5 ng/μl pX330-mC

plasmids carrying a Cas9-Cdt1 fusion gene and respective gRNA (Supplementary Table 1) for *Exoc3l* and 10 ng/μl donor DNA were injected into fertilized eggs from C57BL/6J mice (Charles River Laboratories Japan, Yokohama, Japan) in accordance with a previous report [15]. Genotyping PCR of *Exoc3l* mice was performed using BioTaq (Meridian Bioscience, Cincinnati, OH, USA) with the primers listed in Supplementary Table 2.

This study was approved and conducted in accordance with the Regulations for Animal Experimentation of Tsukuba University and Shiga University of Medical Sciences (Approval numbers: 2017-8-6, 2017-11-4, 2020-11-3, 2022-6-3, 2022-10-6, and 2023-4-7).

RNA-seq analysis

scRNA-seq data from E9.5 mouse embryos (E-MTAB-10945) was downloaded from the EMBL European Bioinformatics Institute (https://www.ebi.ac.uk/). After extraction of the wildtype (WT) subset of E9.5 mouse embryos from the scRNA-seq data [16], we performed conventional scRNA-seq processing using Seurat_v4.1.1 by R (https://www.r-project.org/) [16]. The methods of Azzoni *et al.* were adopted for quality control of the dataset and dead cell removal. Briefly, cells were filtered out by the number of features, unique molecular identifier (UMI), and the percentage of mitochondrial gene expression. After normalization of UMI counts to the total counts per cell, the 2,000 most highly variable genes were used to scale the expression and perform principal component (PC) analysis. To find significant PCs, the efficacious PC threshold was calculated by (1) the cumulative %stdev of PCs >90 and %variation associated with PCs <5, and (2) the last point of change of %PC variation >0.1. We selected the minimum value between (1) and (2) as the significant PC for this analysis. After preprocessing for clustering, a k-NN graph was constructed by Louvain clustering using the top 12 PCs, and a UMAP was drawn. For doublet removal, we used DoubletFinder [17]. Cell types were annotated by each cell lineage marker described previously [16].

Gene expression levels of *Exoc3*, *Exoc3l*, *Exoc3l2*, *Exoc3l3*, and *Exoc3l4* in adult mouse tissues were obtained using transcripts per million (TPM) values of C57BL/6, CD1, and DBA/2J mice obtained from the Expression atlas database (https://www.ebi.ac.uk/gxa/home) [18].

Reverse transcription-quantitative PCR

Total RNA was extracted using TRIzol® (Invitrogen, Waltham, MA, USA), followed by cDNA synthesis using a ReverTra Ace kit (Toyobo, Osaka, Japan) in accordance with the manufacturers' instructions. Real-time PCR was

performed using Thunderbird SYBR qPCR Mix (Toyobo) by StepOnePlus™ (Thermo Fisher Scientific, Waltham, MA, USA). Data were normalized to *Gapdh* expression. Primer sequences are listed in Supplementary Table 3.

Immunohistochemistry of embryos

Mice were sacrificed by cervical dislocation. Embryos were dissected out and fixed in 4% paraformaldehyde (PFA) for 2 h at 4°C, as described previously [19]. For whole mount immunohistochemistry, after washing in PBS, embryos were permeabilized in 0.5% Triton X-100 (Sigma-Aldrich, St. Louis, MO, USA) in PBS for 30 min at 4°C. Permeabilized embryos were blocked in blocking solution containing 2% bovine serum albumin (Sigma-Aldrich) and 0.01% Tween 20 (Nacalai Tesque, Inc., Kyoto, Japan) in PBS (0.01% PBST) for 1 h at room temperature (RT). The embryos were incubated with a rat anti-PECAM1 antibody (1:200; BD Pharmingen, Franklin Lakes, NJ, USA) and anti-red fluorescent protein (RFP) rabbit polyclonal antibody (1:500; MBL Inc., Tokyo, Japan). After three washes with 0.2% PBST, embryos were incubated with secondary antibodies (Donkey anti-Rat IgG (H+L) Highly Cross-Adsorbed Secondary Antibody, Alexa Fluor™ 488 and Donkey anti-Rabbit IgG (H+L) Highly Cross-Adsorbed Secondary Antibody, Alexa Fluor™ 594) (Invitrogen) for 1 h at RT. Embryos were then washed three times with 0.2% PBST. Nuclei were counterstained with 10 μg/ml Hoechst 33342 (Molecular Probes Inc., Eugene, OR, USA) for 10 min at RT. Images were acquired under a BZ-9000 microscope (Keyence, Osaka, Japan) and processed using Adobe Photoshop (Adobe Systems, San Jose, CA, USA).

Evaluation of angiogenesis during embryogenesis

WT and *Exoc3l* KO embryos at 9.5 dpc (20–25 somite stage) were chosen for evaluation. Total area, vascular area, and vascular length were calculated by Fiji (version 2.3.0/ 1.53q software) [20]. Total area was the dorsal area from the level of the posterior edge of the otocyst to the anterior edge of the third somite pair. Vascular area was the PECAM1-positive area. Vascular length was the total length of PECAM1-positive vessels.

Immunostaining of whole mount retinas

Whole-mounted retinas were stained in accordance with a previous report [21]. Briefly, enucleated eyes of P7 WT and *Exoc3l* KO mice were fixed for 20 min in 4% PFA at RT. A small hole was made in the cornea using a 27 G needle, and a circular incision was introduced using fine scissors. Subsequently, retinal cups were dissected from the eyes and post-fixed for 30 min in 4% PFA at 4°C. Primary antibodies were rabbit anti-neuron-glial antigen-2 (NG2) (1:200; Millipore-Sigma, St. Louis, MO, USA) and hamster anti-PECAM1 (1:1000; Abcam, Cambridge, UK). Secondary antibodies were species-specific secondary antibodies (Jackson ImmunoResearch Laboratories, Inc., West Grove, PA, USA) or streptavidin coupled to Alexa Fluor dyes (Invitrogen). Nuclei were counterstained with 10 μg/ml Hoechst 33342 (Molecular Probes Inc., Eugene, OR, USA) for 10 min at RT. Whole retinas were mounted using ProLong™ Gold Antifade Mountant (Thermo Fisher Scientific). Confocal images were acquired under a TCS-SP8 microscope (Leica, Wetzlar, Germany). Fluorescence was produced using a 552 nm laser for Cy3, a 488 nm laser for Alexa Fluor 488, and a 405 nm UV laser for Hoechst 33342 and 4',6-diamidino-2-phenylindole (DAPI). Z-stack images were obtained every 5 μm. The hybrid detector HyD (Leica) was used for signal amplification. Projection images were created by 3D viewer software (Leica) from z-stack images.

Measurement of the plasma cholesterol concentration

Blood samples were collected from tail veins of 7–8-week-old male and female mice and transferred into tubes containing 10 U heparin (Nipro Pharma Corp., Osaka, Japan), followed by centrifugation at 1,000 × *g* for 15 min at 4°C to separate the plasma. Plasma cholesterol concentrations were measured using an E-test WAKO kit (Fujifilm Wako Pure Chemical Corp., Osaka, Japan) in accordance with the manufacturer's instructions.

Glucose tolerance test

A glucose tolerance test was performed as described previously [22]. Briefly, 10-week-old male WT and KO mice were fasted overnight (16–18 h) and then intraperitoneally injected with a D-glucose solution (2 g/kg BW). Blood samples were collected at 0min and 15min. Blood glucose levels were measured using a Glutest Neo alpha (Sanwa Kagaku Kenkyusho Co., Ltd., Aichi, Japan), and plasma insulin levels were determined by an ELISA (#M1104; Morinaga, Tokyo, Japan). Homeostatic model assessment of insulin resistance (HOMA-IR) an index of insulin resistance was calculated using the following formula [23]: HOMA-IR = fasting blood glucose (mg/dl) × fasting plasma insulin (mU/l) / 405.

Biochemical testing

10-week-old female WT and KO mice were euthanized by cervical spine fracture dislocation. Whole blood from the heart was collected in a heparin-Li-coated tube

(#450536; Greiner, Tokyo, Japan) and blood plasma was measured by a VetScan VS2 (Medical space SPACE, Saitama, Japan) with MultiRoter 1 General Diagnostic Panel A (Zoetis JAPAN, Tokyo, Japan).

Blood cell counting

10-week-old female WT and KO mice were euthanized by cervical spine fracture dislocation. Whole blood from the heart was collected in an EDTA-coated tube (# 2909000; Tokyo Garasu Kikai, Tokyo, Japan) and analyzed by a Celltac α (Nihon Kohden, Tokyo, Japan).

Statistical analysis

The unpaired Student's *t*-test, one-way ANOVA with the post hoc Tukey-Kramer test, and two-way ANOVA with the post hoc Sidak test were used for statistical analysis. Data are presented as means ± SEM or means ± SD. Statistical significance was determined at $P<0.05$.

The observed values of crossing the heterozygotes were compared with the expected values by the chi-squared test with $P<0.05$ considered significant.

Results and Discussion

Generation of *Exoc3l* knockout mice

Previously, we identified *Exoc3l* as an endothelial cell-enriched gene by microarray analysis [14]. Because scRNA-seq analysis reveals gene expression patterns and specificity at higher resolution than microarray, we re-examined endothelial cell expression of *Exoc3l* using a public database of scRNA-seq data from E9.5 mouse embryos [16]. *Exoc3l* was confirmed to be expressed moderately in cluster 6 (hemato/endothelial cells) and 10 (endothelium), indicating that *Exoc3l* was expressed in a subset of endothelial cells (Supplementary Figs. 1a–c). *Exoc3l* was also expressed widely in tissues in adult mice (Supplementary Fig. 1d).

To examine the physiological function of *Exoc3l*, we designed two gRNAs to knock-in a *tdTomato* cassette into the *Exoc3l* locus and obtained alleles: a *tdTomato* knock-in allele and Δ allele lacking the entire coding sequence (Fig. 1a). We confirmed targeted knock-in of *tdTomato* into the *Exoc3l* locus and targeted deletion of the Δ allele (Fig. 1b) with respective primer sets to detect 5′ and 3′ regions. Furthermore, we sequenced the exon2 and *tdTomato* of the knock-in allele and confirmed the reading frame (data not shown).

When *Exoc3l* heterozygotes were crossed, *Exoc3l* KO mice were born and survived at least until 8 weeks at the expected Mendelian ratio (Fig. 1c). Body weight and the results regarding biochemical testing and blood cell counts from WT and KO were comparable (Fig. 1d and
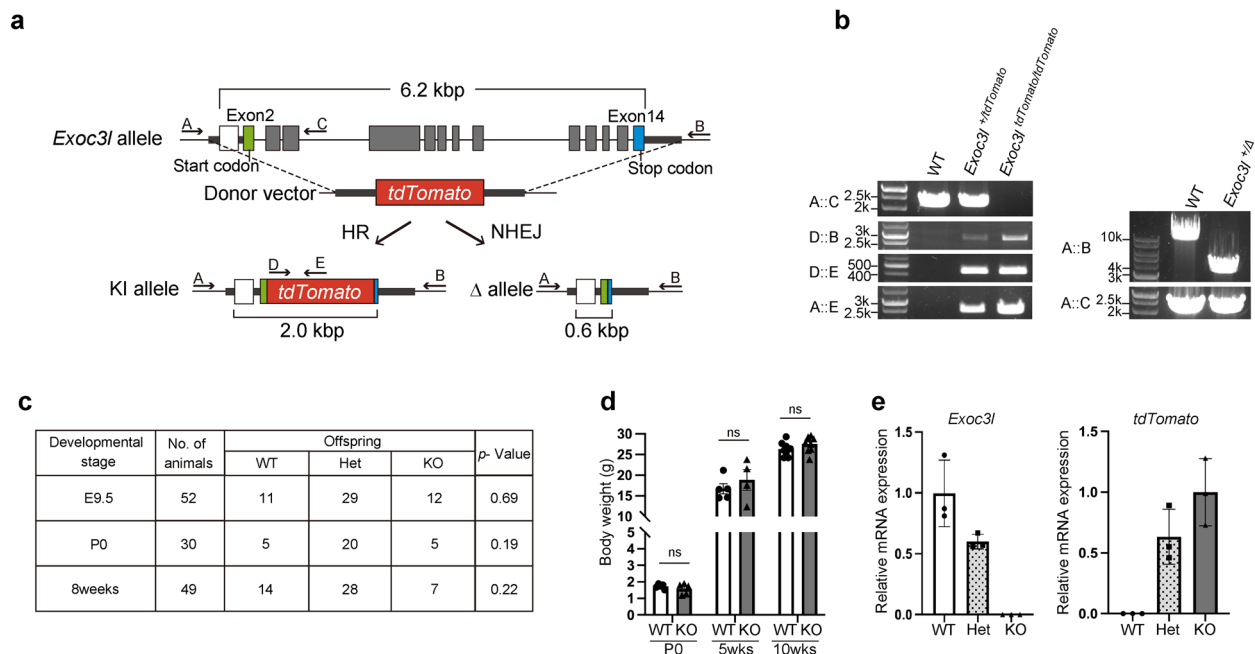
Fig. 1. Generation of *Exoc3l* KO mice. (a) Schematic representation of *Exoc3l* mutant alleles in mice. HR: homologous recombination; KI: knock-in. NHEJ; Non-homologous end-joining, KI; knock-in. (b) Genotyping PCR of *Exoc3l*+/tdTomato, *Exoc3l* tdTomato/tdTomato and *Exoc3l* +/Δ in mice. A–E indicate PCR primers. WT band at 10kb in *Exoc3l* +/Δ in mice was not amplified efficiently under a competitive condition. (c) Table showing the Mendelian ratios of E9.5, P0, and 8-week-old mice. (d) Body weight of *Exoc3l* WT and mutant mice. P0: n=5, 5weeks; WT: n=5, KO: n=4, 10weeks: n=9 (e) Relative mRNA expression of *Exoc3l* and *tdTomato* in the adult tail of 8weeks WT, *Exoc3l*+/tdTomato and *Exoc3l* tdTomato/tdTomato (n=3). Data are presented as means ± SEM (d) or means ± SD (e). ns: not significant. *P*-values were determined using the unpaired Student's *t*-test.

Supplementary Fig. 2). Endogenous *Exoc3l* mRNA was undetectable in *Exoc3l* KO mice, while *tdTomato* mRNA was detectable in *Exoc3l+/tdTomato* KI and *Exoc3l td-Tomato/tdTomato* KI mice (Fig. 1e). However, tdTomato fluorescence was undetectable under a microscope, whereas strong red fluorescence was observed in blood vessels of *Flt1-tdsRed* BAC Tg mice as a positive control (Supplementary Fig. 3) [24]. Although we tried to enhance the tdTomato signal using an antibody against RFP, we did not observe any detectable signal, suggesting that tdTomato expression level may be low.

Angiogenesis during embryogenesis and the postnatal stage

Because we previously identified *Exoc3l* as a critical endothelial cell gene in cultured HUVECs, we evaluated angiogenesis during embryonic development by immunohistochemistry of PECAM1, an endothelial cell marker (Fig. 2a). The PECAM1 staining pattern of *Exoc3l* KO embryos at E9.5 were indistinguishable from those of WT embryos (Fig. 2a). We measured the angiogenic region of the dorsal area, which underwent drastic angiogenesis (highlighted by dotted lines in Fig. 2a), and found no significant difference between WT and *Exoc3l* KO embryos (Fig. 2b).

Retinal angiogenesis starts after birth and is an ideal model to evaluate postnatal angiogenesis [3]. We performed immunohistochemistry with antibodies against PECAM1 and NG2, a pericyte marker, in the retinas of WT and *Exoc3l* KO mice at P7 (Fig. 3a). Radial growth, the distance from the center to the vascular front, the number of filopodia at the vascular front, and pericyte coverage were comparable, indicating that *Exoc3l* KO mice had no apparent vascular defect at E9.5 or retinal vascular defect at P7 (Fig. 3b).

Previous reports indicate that the pathological angiogenesis such as tumour angiogenesis involves different molecular mechanism from normal angiogenesis [2], thus it will be interesting to investigate whether *Exoc3l* plays a role in tumour angiogenesis.

Cholesterol level and insulin secretion

Although *Exoc3l* mice did not show significant phenotype in embryonic angiogenesis and postnatal retinal
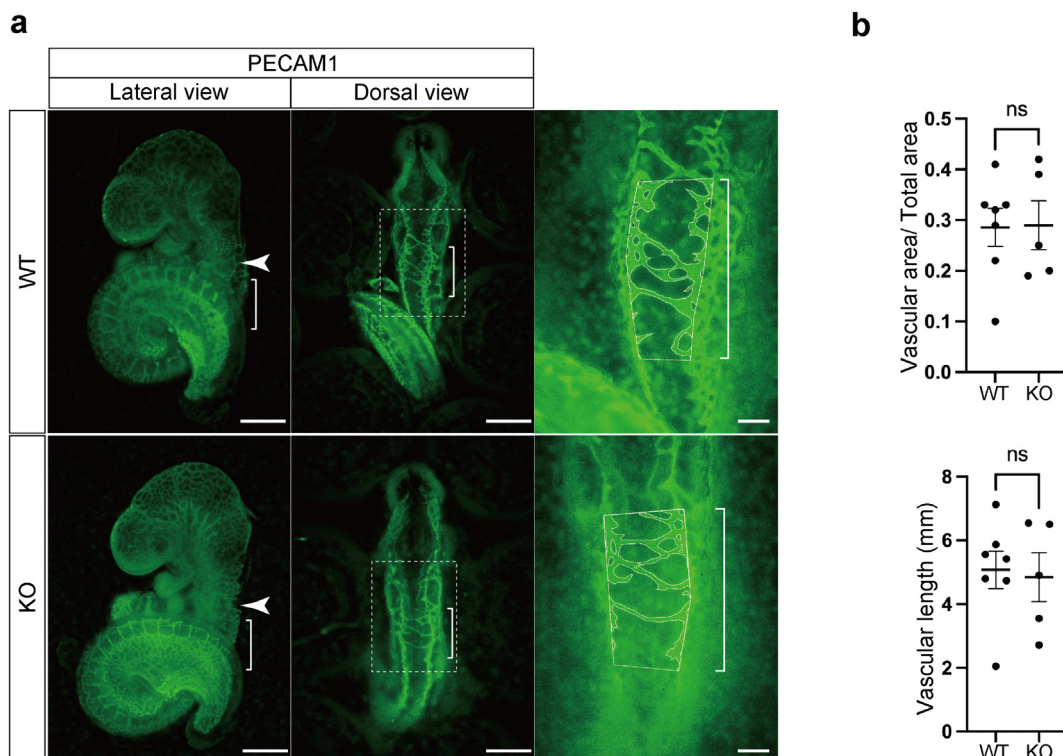
Fig. 2. Embryonic angiogenesis in *Exoc3l* KO mice. (a) Whole mount PECAM1 immunostaining of WT and *Exoc3l* KO embryos at 9.5 dpc (20–25 somite stage). A higher magnification of the dotted square is shown in the right. Scale bars in the lateral view, dorsal view, and higher magnification indicate 500 μm, 500 μm, and 100 μm, respectively. The vascular area was measured by Fiji software. Total area was measured from the bottom of the otocyst to the third somite pair. Vascular area was the area obtained by subtracting the non-vascular area from the total area. Vascular length indicates the perimeter of the vascular area. (b) Quantification of the vascular area and Vascular length in the back region of mouse embryo at E9.5 WT (n=7), KO (n=5) Data are means ± SEM. ns: not significant. *P*-values were determined using the unpaired Student's *t*-test.
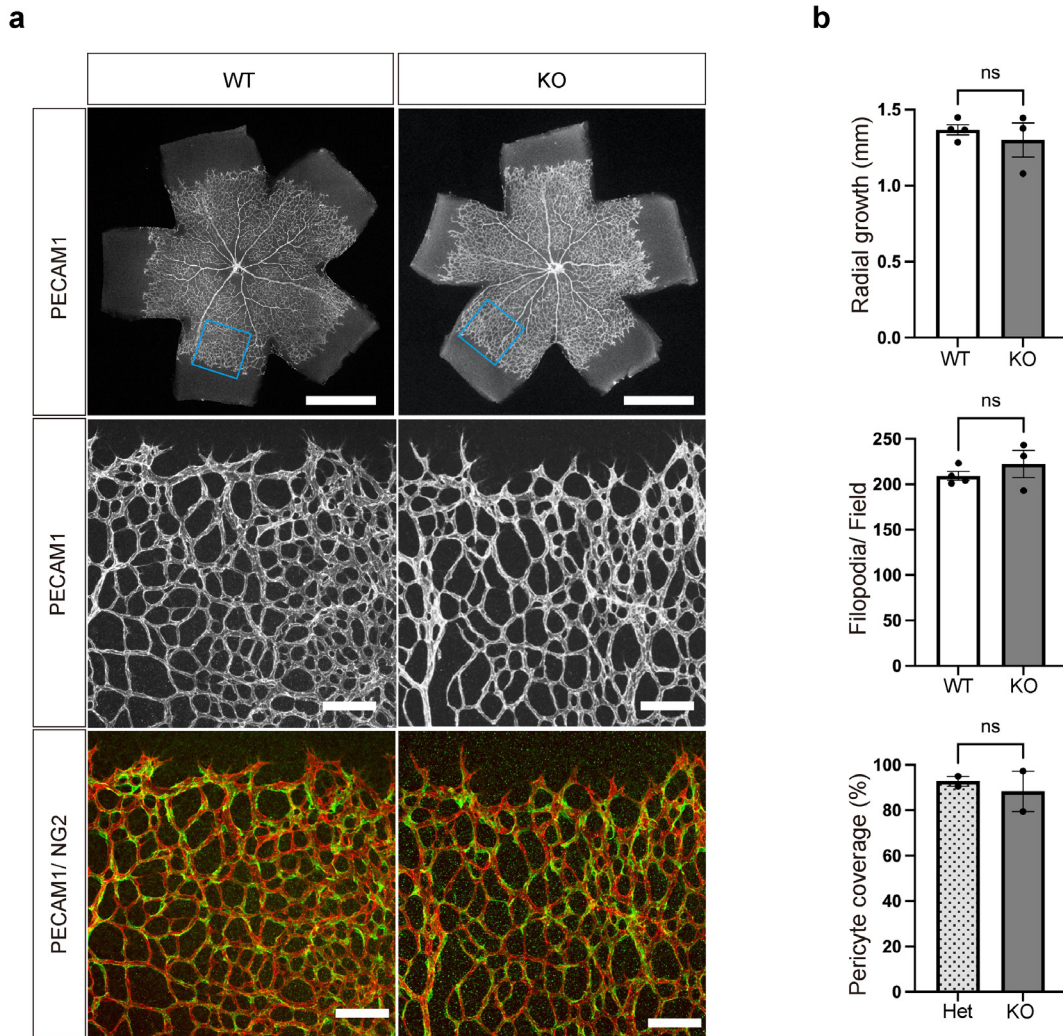
Fig. 3. Retinal angiogenesis in *Exoc3l* KO neonates. (a) Evaluation of retinal angiogenesis in *Exoc3l* KO mice at P7. Scale bars in the whole retina and magnified images indicate 1 mm and 100μm, respectively. (b) Radial outgrowth, filopodia number, and pericyte coverage of WT (n=4), *Exoc3l* hetero KI (n=2), and *Exoc3l* KO (n=3) neonates. ns: not significant. *P*-values were determined using the unpaired Student's *t*-test.

angiogenesis, several reports have suggested that *Exoc3l* plays other physiological roles than vascular development. Lanktree *et al*. reported that *Exoc3l* is associated with cholesterol homeostasis on the basis of linkage analysis [12]. Therefore, we determined whether *Exoc3l* KO mice showed any alteration in the total level of cholesterol (Fig. 4a). Concentrations of plasma cholesterol were comparable among WT, *Exoc3l* heterozygous, and *Exoc3l* KO mice.

Saito *et al.* reported that *Exoc3l* may be implicated in insulin secretion from an insulinoma cell line [13]. Therefore, we investigated whether *Exoc3l* played a role in insulin secretion (Figs. 4b–d). The glucose tolerance test indicated no significant difference between WT and *Exoc3l* KO mice (Fig. 4b). The level of plasma insulin and insulin resistance were also comparable between WT and *Exoc3l* KO mice (Figs. 4c and d). Taken to-

gether, *Exoc3l* KO mice did not show any significant phenotype in terms of vascular development, cholesterol homeostasis, or insulin secretion. The reason why *Exoc3l* KO mice did not show any significant phenotype in these biological processes was unclear, but it may be due to the compensation by the other members, because there are four other similar members, EXOC3 (also called SEC6), EXOC3l2, EXOC3l3 and EXOC3l4 (Supplementary Fig. 4a). Exoc3l is a highly conserved protein between mouse and human (Supplementary Fig. 4b), suggesting a role in both species.

In summary, *Exoc3l* KO mice did not show any significant phenotypes in vascular development, cholesterol homeostasis, or insulin secretion.
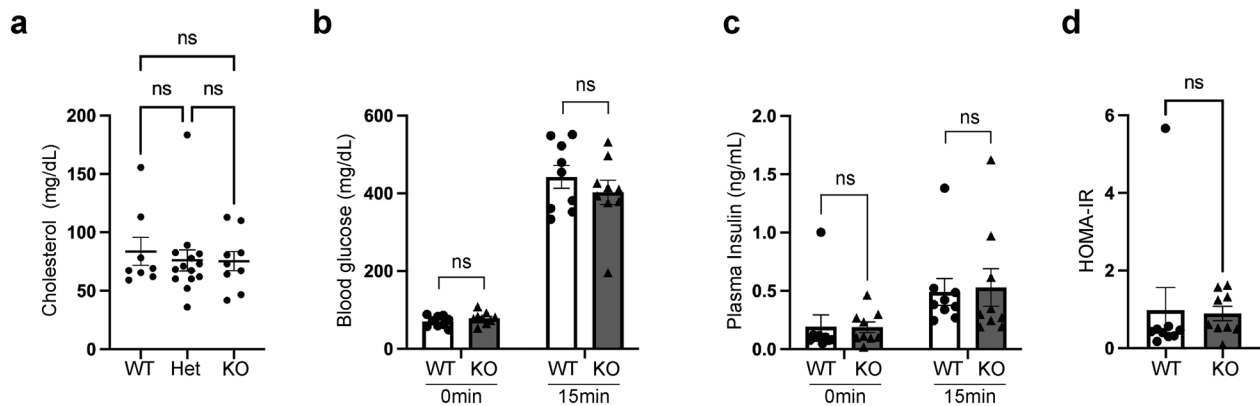
Fig. 4. Metabolic parameters of *Exoc3l* KO mice. (a) Concentrations of plasma cholesterol in controls (WT, n=8), heterozygotes (Het, n=14), and homozygotes (KO, n=9) of 7-8-week-old male and female. (b) Glucose tolerance test comparing 10-week-old male WT and KO mice (2 g glucose/kg i.p.; n=9). (c) Plasma insulin levels of 10-week-old male WT and KO mice at baseline and 15 min after glucose administration (2 g glucose/kg i.p.; n=9). (d) HOMA-IR index of 10-week-old male WT and KO mice (n=9). Data are presented as means ± SEM. ns: not significant. *P*-values were determined using the unpaired Student's *t*-test (d), one-way ANOVA with the post hoc Tukey-Kramer test (a), and two-way ANOVA with the post hoc Sidak test (b, c).

Author Contributions

M.E. conceived the project. S.T. and M.E. wrote the manuscript. S.T., E.O., Y.I., K.N., A.S., C.W., M.M., S.M., S.T-F., T.T., F.S., S.T. and S.M. performed experiments. S.T., E.O., Y.I., K.N., A.S., C.W., M.M., S.M., H.O., E.N., M.O., K.M., and M.E. analyzed data. M.E. supervised the research. All authors contributed to editing the manuscript.

Declaration of Interests

None.

Acknowledgments

References

1. Adams RH, Alitalo K. Molecular regulation of angiogenesis and lymphangiogenesis. Nat Rev Mol Cell Biol. 2007; 8: 464–478. [Medline] [CrossRef]
2. Carmeliet P, Jain RK. Molecular mechanisms and clinical applications of angiogenesis. Nature. 2011; 473: 298–307. [Medline] [CrossRef]
3. Gerhardt H, Golding M, Fruttiger M, Ruhrberg C, Lundkvist A, Abramsson A, et al. VEGF guides angiogenic sprouting utilizing endothelial tip cell filopodia. J Cell Biol. 2003; 161: 1163–1177. [Medline] [CrossRef]
4. Langevin J, Morgan MJ, Sibarita JB, Aresta S, Murthy M, Schwarz T, et al. Drosophila exocyst components Sec5, Sec6, and Sec15 regulate DE-Cadherin trafficking from recycling endosomes to the plasma membrane. Dev Cell. 2005; 9: 365–376. [Medline] [CrossRef]
5. Xiong X, Xu Q, Huang Y, Singh RD, Anderson R, Leof E, et al. An association between type Iγ PI4P 5-kinase and Exo70 directs E-cadherin clustering and epithelial polarization. Mol Biol Cell. 2012; 23: 87–98. [Medline] [CrossRef]
6. Jafar-Nejad H, Andrews HK, Acar M, Bayat V, Wirtz-Peitz F, Mehta SQ, et al. Sec15, a component of the exocyst, promotes notch signaling during the asymmetric division of Drosophila sensory organ precursors. Dev Cell. 2005; 9: 351–363. [Medline] [CrossRef]
7. Friedrich GA, Hildebrand JD, Soriano P. The secretory protein Sec8 is required for paraxial mesoderm formation in the mouse. Dev Biol. 1997; 192: 364–374. [Medline] [CrossRef]
8. Murthy M, Garza D, Scheller RH, Schwarz TL. Mutations in the exocyst component Sec5 disrupt neuronal membrane traffic, but neurotransmitter release persists. Neuron. 2003; 37: 433–447. [Medline] [CrossRef]
9. Fogelgren B, Polgar N, Lui VH, Lee AJ, Tamashiro KK, Napoli JA, et al. Urothelial Defects from Targeted Inactivation of Exocyst Sec10 in Mice Cause Ureteropelvic Junction Obstructions. PLoS One. 2015; 10: e0129346. [Medline] [CrossRef]
10. Mizuno S, Takami K, Daitoku Y, Tanimoto Y, Dinh TT, Mizuno-Iijima S, et al. Peri-implantation lethality in mice carrying megabase-scale deletion on 5qc3.3 is caused by Exoc1 null mutation. Sci Rep. 2015; 5: 13632. [Medline] [CrossRef]
11. Watanabe C, Shibuya H, Ichiyama Y, Okamura E, Tsukiyama-Fujii S, Tsukiyama T, et al. Essential Roles of *Exocyst Complex Component 3-like 2* on Cardiovascular Development in Mice. Life (Basel). 2022; 12: 1730. [Medline]
12. Lanktree MB, Elbers CC, Li Y, Zhang G, Duan Q, Karczewski KJ, et al. Genetic meta-analysis of 15,901 African Americans identifies variation in EXOC3L1 is associated with HDL concentration. J Lipid Res. 2015; 56: 1781–1786. [Medline] [CrossRef]
13. Saito T, Shibasaki T, Seino S. Involvement of Exoc3l, a protein structurally related to the exocyst subunit Sec6, in insulin secretion. Biomed Res. 2008; 29: 85–91. [Medline] [CrossRef]
14. Takase H, Matsumoto K, Yamadera R, Kubota Y, Otsu A, Suzuki R, et al. Genome-wide identification of endothelial cell-enriched genes in the mouse embryo. Blood. 2012; 120: 914–923. [Medline] [CrossRef]
15. Mizuno-Iijima S, Ayabe S, Kato K, Matoba S, Ikeda Y, Dinh

TTH, et al. Efficient production of large deletion and gene fragment knock-in mice mediated by genome editing with Cas9-mouse Cdt1 in mouse zygotes. Methods. 2021; 191: 23–31. [Medline] [CrossRef]

16. Azzoni E, Frontera V, Anselmi G, Rode C, James C, Deltcheva EM, et al. The onset of circulation triggers a metabolic switch required for endothelial to hematopoietic transition. Cell Rep. 2021; 37: 110103. [Medline] [CrossRef]

17. McGinnis CS, Murrow LM, Gartner ZJ. DoubletFinder: Doublet Detection in Single-Cell RNA Sequencing Data Using Artificial Nearest Neighbors. Cell Syst. 2019; 8: 329–337.e4. [Medline] [CrossRef]

18. Petryszak R, Keays M, Tang YA, Fonseca NA, Barrera E, Burdett T, et al. Expression Atlas update--an integrated database of gene and protein expression in humans, animals and plants. Nucleic Acids Res. 2016; 44:(D1): D746–D752. [Medline] [CrossRef]

19. Ema M, Yokomizo T, Wakamatsu A, Terunuma T, Yamamoto M, Takahashi S. Primitive erythropoiesis from mesodermal precursors expressing VE-cadherin, PECAM-1, Tie2, endoglin, and CD34 in the mouse embryo. Blood. 2006; 108: 4018–4024. [Medline] [CrossRef]

20. Schindelin J, Arganda-Carreras I, Frise E, Kaynig V, Longair M, Pietzsch T, et al. Fiji: an open-source platform for biological-image analysis. Nat Methods. 2012; 9: 676–682. [Medline] [CrossRef]

21. Ichiyama Y, Obata S, Saishin Y, Sawada O, Kakinoki M, Sawada T, et al. The systemic antiangiogenic effect of intravitreal aflibercept injection in a mouse model of retinopathy of prematurity. FASEB J. 2021; 35: e21390. [Medline] [CrossRef]

22. Nishi K, Sato Y, Ohno M, Hiraoka Y, Saijo S, Sakamoto J, et al. Nardilysin Is Required for Maintaining Pancreatic β-Cell Function. Diabetes. 2016; 65: 3015–3027. [Medline] [CrossRef]

23. Miyagawa K, Kondo T, Goto R, Matsuyama R, Ono K, Kitano S, et al. Effects of combination therapy with vildagliptin and valsartan in a mouse model of type 2 diabetes. Cardiovasc Diabetol. 2013; 12: 160. [Medline] [CrossRef]

24. Matsumoto K, Azami T, Otsu A, Takase H, Ishitobi H, Tanaka J, et al. Study of normal and pathological blood vessel morphogenesis in Flt1-tdsRed BAC Tg mice. Genesis. 2012; 50: 561–571. [Medline] [CrossRef]